Original Article

Multiparametric simultaneous hybrid ^{18}F-fluorodeoxyglucose positron emission tomography/magnetic resonance imaging (^{18}F-FDG PET/MRI) incorporating intratumoral and peritumoral regions for grading of glioma

Ping Liu[1#], Yu-Ping Zeng[2,3#], Hong Qu[1], Wan-Yi Zheng[1], Tian-Xing Zhou[4], Li-Feng Hang[4], Gui-Hua Jiang[1,4,5]

[1]Department of Medical Imaging, The Affiliated Guangdong Second Provincial General Hospital, Jinan University, Guangzhou, China; [2]Department of Medical Imaging, Ganzhou People's Hospital, Ganzhou, China; [3]Department of Nuclear Medicine, Guangzhou Universal Medical Imaging Diagnostic Center, Guangzhou, China; [4]Department of Medical Imaging, Guangdong Second Provincial General Hospital, Guangzhou, China; [5]Guangzhou Key Laboratory of Molecular Functional Imaging and Artificial Intelligence for Major Brain Diseases, The Affiliated Guangdong Second Provincial General Hospital, Jinan University, Guangzhou, China

Contributions: (I) Conception and design: P Liu, GH Jiang; (II) Administrative support: GH Jiang; (III) Provision of study materials or patients: YP Zeng; (IV) Collection and assembly of data: YP Zeng, WY Zheng; (V) Data analysis and interpretation: YP Zeng, H Qu, TX Zhou, LF Hang; (VI) Manuscript writing: All authors; (VII) Final approval of manuscript: All authors.

[#]These authors contributed equally to this work and should be considered as co-first authors.

Correspondence to: Gui-Hua Jiang, MD, PhD. Department of Medical Imaging, The Affiliated Guangdong Second Provincial General Hospital, Jinan University, #466 Xingang Middle Road, Haizhu District, Guangzhou 510317, China; Department of Medical Imaging, Guangdong Second Provincial General Hospital, Guangzhou 510317, China; Guangzhou Key Laboratory of Molecular Functional Imaging and Artificial Intelligence for Major Brain Diseases, The Affiliated Guangdong Second Provincial General Hospital, Jinan University, Guangzhou 510317, China. Email: 13828472201@163.com.

Background: Preoperative grading gliomas is essential for therapeutic clinical decision-making. Current non-invasive imaging modality for glioma grading were primarily focused on magnetic resonance imaging (MRI) or positron emission tomography (PET) of the tumor region. However, these methods overlook the peritumoral region (PTR) of tumor and cannot take full advantage of the biological information derived from hybrid-imaging. Therefore, we aimed to combine multiparameter from hybrid ^{18}F-fluorodeoxyglucose (^{18}F-FDG) PET/MRI of the solid component and PTR were combined for differentiating high-grade glioma (HGG) from low-grade glioma (LGG).

Methods: A total of 76 patients with pathologically confirmed glioma (41 HGG and 35 LGG) who underwent simultaneous ^{18}F-FDG PET, arterial spin labelling (ASL), and diffusion-weighted imaging (DWI) with hybrid PET/MRI were retrospectively enrolled. The relative maximum standardized uptake value ($rSUV_{max}$), relative cerebral blood flow (rCBF), and relative minimum apparent diffusion coefficient ($rADC_{min}$) for the solid component and PTR at different distances outside tumoral border were compared. Receiver operating characteristic (ROC) curves were applied to assess the grading performance. A nomogram for HGG prediction was constructed.

Results: HGGs displayed higher $rSUV_{max}$ and rCBF but lower $rADC_{min}$ in the solid component and 5 mm-adjacent PTR, lower $rADC_{min}$ in 10 mm-adjacent PTR, and higher rCBF in 15- and 20-mm-adjacent PTR. $rSUV_{max}$ in solid component performed best [area under the curve (AUC) =0.865] as a single parameter for grading. Combination of $rSUV_{max}$ in the solid component and adjacent 20 mm performed better (AUC =0.881). Integration of all 3 indicators in the solid component and adjacent 20 mm performed the best (AUC

=0.928). The nomogram including $rSUV_{max}$, rCBF, and $rADC_{min}$ in the solid component and 5-mm-adjacent PTR predicted HGG with a concordance index (C-index) of 0.906.

Conclusions: Multiparametric ^{18}F-FDG PET/MRI from the solid component and PTR performed excellently in differentiating HGGs from LGGs. It can be used as a non-invasive and effective tool for preoperative grade stratification of patients with glioma, and can be considered in clinical practice.

Keywords: Glioma; ^{18}F-fluorodeoxyglucose positron emission tomography/magnetic resonance imaging (^{18}F-FDG PET/MRI); arterial spin labelling (ASL); diffusion-weighted imaging (DWI); peritumoral regions (PTRs)

Submitted Feb 12, 2024. Accepted for publication May 30, 2024. Published online Jun 11, 2024.
doi: 10.21037/qims-24-280
View this article at: https://dx.doi.org/10.21037/qims-24-280

Introduction

Optimized management of glioma, the most common primary brain tumor, remains a major global concern (1). According to the 2021 World Health Organization (WHO) classification of central nervous system tumors (2), the diagnosis of gliomas should be an overall "integrated" diagnosis that is reached according to the histopathological denomination, grade, and molecular information. The imaging and neuroradiologist play pivotal roles in glioma diagnosis; the neuroradiologist raises an initial diagnosis of glioma, and the results are confirmed further by histopathological exam, whereas the imaging provides the information of lesion localization, disease extent, and aids tumor grading and surgical planning (3). Patient survival varies greatly depending on tumor grade, with high-grade glioma (HGG, grade 3+4) having a very high mortality rate (e.g., 5-year survival rate <5%), nevertheless, low-grade glioma (LGG, grade 1+2) achieves a survival rate as high as 80% (4). Additionally, the treatment regimens including the degree of resection, postsurgical radiation, or temozolomide combined with radiation are also implemented according to the glioma's grade. Therefore, accurate pre-operative grading of glioma is critical for clinical decision-making in order to maximize prognosis and patient-tailored precision medicine; however, post-operative histopathological assessment remains the standard for grading gliomas (5). Some patients cannot tolerate surgery or biopsy, in addition, the pathological diagnosis from stereotactic biopsy or surgical resection may be inaccurate due to the tissue heterogeneity and sampling bias (6).

Conventional or advanced magnetic resonance imaging (MRI) have been used to grade gliomas for decades. However, its performance in clinical practice remains unsatisfactory (7). As pathophysiological alterations in tumors are closely associated with aberrant vascularization, hemodynamic imaging, particularly arterial spin labelling (ASL), has been employed to grade glioma due to its advantage of not requiring a tracer (8). Recently, ASL was promoted for employment as a routine clinical setting for glioma (9). Diffusion-weighted imaging (DWI) is a classical and well-known technology for glioma evaluation, but there are no reliable and uniformly accepted threshold values to properly establish grades. Therefore, the value of single imaging techniques remains limited for identifying HGG. Combination of DWI-derived apparent diffusion coefficient (ADC) and ASL has been recommended to simultaneously assess the cellular and vascular properties of gliomas and are viewed as useful biomarkers for grading (10-12). Multiparametric MRI show greater potential in determination of HGGs than does single parameter, but the metabolic behavior of tumors was considered as another valuable biomarker for glioma evaluation.

Positron emission tomography (PET) can visualize biological processes such as cell proliferation, membrane biosynthesis, and glucose consumption by employing various tracers, and thus it has been recommended as standard framework in clinical practice to assist in the management of gliomas (13,14). PET can identify highly metabolically active tissue by measuring uptake of fluorodeoxyglucose (FDG) or other radiotracers, and provide additional insight beyond MRI into the biology of gliomas which may facilitate noninvasive grading of glioma (15). Combining PET and MRI can help procure structural, functional, and metabolic information for glioma in a single examination (16-18), showing additional value to each technique employed alone, especially with the hybrid PET/MRI systems. ^{18}F-fluorodeoxyglucose (^{18}F-FDG), a radiopharmaceutical that is most commonly used as PET

tracer for its higher glucose metabolism that tumor cells exhibit compared to healthy tissues (19), shows superior specificity for grading glioma (20,21). Although ^{18}F-fluoro-ethyl-L-tyrosine (FET) has demonstrated higher diagnostic performance for the diagnosis of brain tumor and glioma, it has shown similar performance for distinguishing LGG and HGG in comparison with ^{18}F-FDG (22). Additionally, as ^{18}F-FDG can be applied at all PET sites, we must concede the major convenience of tracer supply in clinical practice. Theoretically, combined parameters from ^{18}F-FDG hybrid PET/MRI may provide sufficient complementary information to improve the grading of gliomas.

Recent studies have found that the peritumoral region (PTR), a region that appears radiologically and macroscopically normal, is crucial for tumor classification (23). Reports have shown that tumor cell infiltration can extend several centimeters beyond the tumor margin (24), thus, a thorough understanding of the actual extent of the region beyond MRI-defined abnormalities is crucial for improving the management of glioma, such as to help determine new therapeutic targets (25). DWI (26) and perfusion imaging (27) have been used to detect alterations in PTR. Combination of ASL, DWI, and ^{18}F-FDG PET parameters from the enhancing tumors and PTR has shown good performance to differentiate HGGs from lymphomas (28). However, multiple parameters derived from the solid component and PTR have not been used for grading gliomas. We hypothesized that multiple parameters derived from ^{18}F-FDG PET/MRI of multiple tumoral regions would improve the grading performance.

Therefore, we combined multiparameters derived from hybrid ^{18}F-FDG PET/MRI of the solid component and PTR to differentiate LGG from HGG, and expected to provide comprehensive physiological and biochemical information that can potentially improve the accuracy of glioma grading. We present this article in accordance with the TRIPOD reporting checklist (available at https://qims.amegroups.com/article/view/10.21037/qims-24-280/rc).

Methods

Patients

The ^{18}F-FDG PET/MRI examination was approved by the Institutional Review Board of Guangzhou Universal Medical Imaging Diagnostic Center (No. 003/2019) and conducted in accordance with the Declaration of Helsinki (as revised in 2013). All patients signed an informed consent form for the ^{18}F-FDG PET/MRI examination. Patients with histologically confirmed gliomas and who had undergone pre-treatment brain ^{18}F-FDG PET/MRI between May 2019 and March 2023 at Guangzhou Universal Medical Imaging Diagnostic Center were retrospectively enrolled. The data applied in this study were exempted from ethical review due to the retrospective nature.

Totally, 131 patients were initially enrolled. The inclusion criteria were as follows: (I) complete ^{18}F-FDG PET/MRI data including T1-weighted imaging (T1WI), T2-weighted imaging (T2WI), T2-weighted fluid-attenuated inversion recovery (T2-FLAIR), DWI, ASL, and ^{18}F-FDG PET before surgery; (II) histopathologically-confirmed glioma without other brain tumors; and (III) no history of treatment, including steroid treatment, radiotherapy, or chemotherapy. The exclusion criteria were as follows: (I) ambiguous grade, especially between grade II and III; (II) incomplete exam or poor image quality (such as motion artifacts); (III) unusual glioma location (e.g., pineal gland, close to the lateral ventricle which may be contaminated by cerebrospinal fluid) that could influence data analysis; (IV) lesions below 5–10 mm; and (V) obvious hemorrhage or large amount of calcification. Tumor grading was based on the 2016 World Health Organization classification, ascertained during operation or via stereotactic brain biopsy. Grades I and II were grouped together as LGG, whereas grade III and IV were grouped together as HGG.

The flowchart for patient enrollment is shown in *Figure 1*. The participants' clinical and conventional imaging features, including age, sex, location, cystic degeneration/necrosis, range of involvement, mass effect, and the detailed histopathology were collected from the hospital electronic system. Finally, 41 patients with HGGs [mean age, 51.54 years (range, 29–79 years)] and 35 patients with LGGs [mean age, 45.06 years (range, 23–69 years)] met the inclusion criteria.

PET/MRI image acquisition

PET/MRI images were obtained on an integrated 3T PET/MRI system (Biograph mMRI; Siemens Healthcare, Erlangen, Germany) with a 12-channel, PET-compatible receiver head coil. All patients had fasting blood glucose level <8.3 mmol/L (150 mg/dL) and had fasted for at least 6 hours prior to examination. Before imaging, FDG was administered intravenously according to the patient's weight, with a standard of 3.70–5.55 MBq/kg. After 40 minutes of uptake in a dimly lit room with eyes open, the patient was positioned for brain imaging.

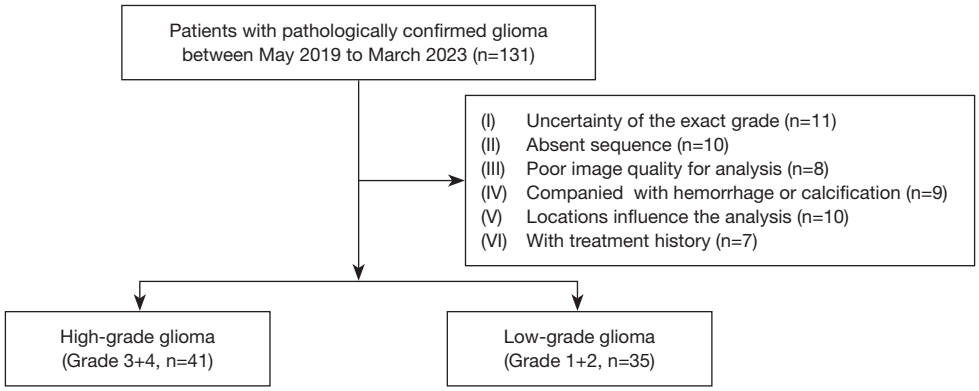

Figure 1 The flowchart of the patient recruitment process.

The comprehensive protocol included the following MRI sequences acquired simultaneously during PET:

(I) 3D-T1WI-magnetization-prepared rapid gradient echo (MPRAGE): repetition time/echo time (TR/TE), 2,000/2.3 ms; slice thickness/gap, 5/1.5 mm; field of view (FOV), 250×250 mm^2; matrix, 256×256;
(II) T2WI: TR/TE, 5,000/91 ms; slice thickness/gap, 5/1.5 mm; FOV, 230×201 mm^2; matrix, 384×307;
(III) T2-FLAIR: TR/TE, 9,000/102 ms; slice thickness/gap, 5/1.5 mm; FOV, 230×201 mm^2; matrix, 256×230;
(IV) Single-shot echo-planar DWI (b=0 and 1,000 s/mm^2): TR/TE, 5,900/85 ms; slice thickness/gap, 5/1.5 mm; FOV, 230×201 mm^2; matrix, 146×146;
(V) ASL: TR/TE, 2,500/13 ms; slice thickness/gap, 8/2 mm; FOV, 256×256 mm^2; matrix, 64×64. The CBF maps were automatically generated after the scan.

Brain PET images were simultaneously acquired with the MRI acquisition without re-positioning. The attenuation correction method of tissue segmentation and iterative reconstruction algorithm with 21 subsets, 3 iterations, and 4 mm (full width at half maximum) post-filtering was used.

Image analysis

Images were transferred to a postprocessing workstation (Syngovia 3.0, Siemens Healthcare, Germany) and independently interpreted by 2 experienced radiologists (P.L. and G.H.J. with 15 and 20 years of experience in neuroradiology, respectively) who were blinded to tumor grade and patient identity. Location, necrosis, and cystic degeneration were qualitatively assessed on conventional MRI. As the relative values, obtained by normalizing the ROI to the normal appearing (contralateral) tissue using mirrored ROI, may help improve accuracy in tumor grading (29). Thus, we used the relative values (the values of ROI divided by the value of the mirrored ROI from the contralateral normal-appearing brain regions) of PET, CBF, and ADC for quantitative assessment. The delineation of the margin was performed by the previous 2 neuroradiologists; any disagreements about the placement of ROIs within each lesion and the definition of the solid component of the glioma were resolved by consensus or with the assistance of a senior radiologist with over 30 years of experience in brain tumor diagnosis. The pipeline of the process of the measurements of multiple parameters in our study are shown in *Figure 2* and as follows:

(I) The cross-section with the largest tumor area and best demarcation of the lesions was chosen, and the T2-FLAIR and T2WI images were used as visual aid.
(II) The solid component of glioma was first identified, on combination of the T2-FLAIR (a slightly higher signal intensity than normal brain tissue but lower than edema) and PET images, PTR with 5, 10, 15, and 20 mm adjacent to the margin of the solid region were defined (*Figure 2A*), 5 round ROIs with a diameter of 5 mm were placed in the solid part without overlap, and the average values were recorded for analysis. Areas adjacent to hemorrhage, vessels, and cystic components were carefully avoided and excluded. Another 4 ROIs were then copy-and-pasted onto the PTR at different distances with 5, 10, 15, and 20 mm adjacent to the margin of the solid region. Additionally, the ROIs were copied into the contralateral normal-appearing tissue as mirrored ROI (*Figure 2B*).
(III) ROIs were copied onto maps of ADC maps (*Figure 2C*), and CBF maps (*Figure 2D*).

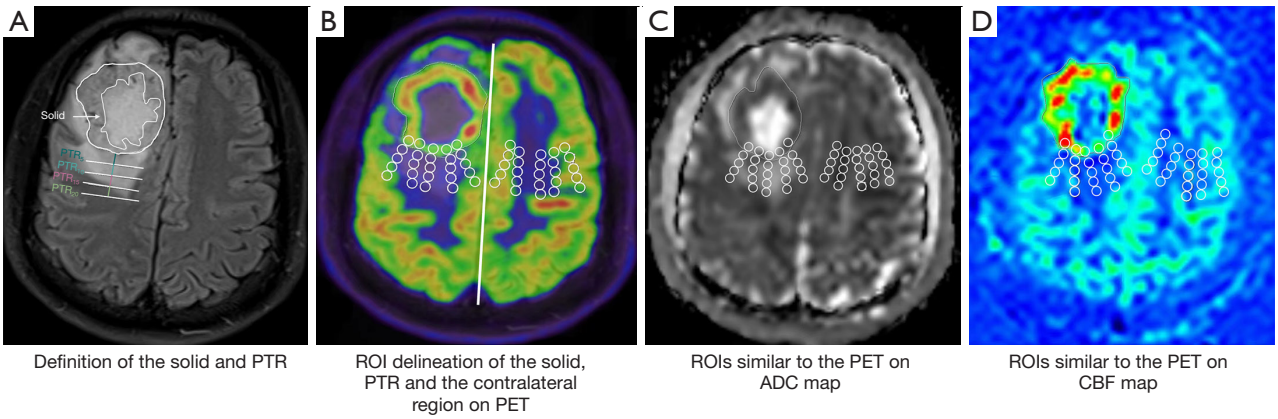

Figure 2 The pipeline of the process of the measurements of multiple parameters from multiple regions. (A) Illustration of the definition of the solid component and PTR with 5, 10, 15, and 20 mm adjacent to the margin of the solid region. (B) The delineation of ROI of the solid component, PTR, and the contralateral region of those ROIs on PET maps. A total of 5 round ROIs with an area of 25 mm^2 are placed in the solid part of the tumor on PET image. The ROIs were copied onto maps of ADC (C), and CBF (D). PTR, peritumoral region; ROI, region of interest; PET, positron emission tomography; ADC, apparent diffusion coefficient; CBF, cerebral blood flow.

(IV) The maximum standardized uptake value (SUV_{max}), CBF, and minimum apparent diffusion coefficient (ADC_{min}) were recorded for each ROI. The relative values of these multiparameters, including relative maximum standardized uptake value ($rSUV_{max}$), relative cerebral blood flow (rCBF), and relative minimum apparent diffusion coefficient ($rADC_{min}$), which were generated by the values of an ROI from the tumor divided by the value of the mirrored ROI, were measured for analysis. Additionally, in order to be interpreted conveniently, $rSUV_{max}$ values from ROIs at distinct locations was recorded as follows: $rSUV_{max\text{-}solid}$, $rSUV_{max\text{-}5}$, $rSUV_{max\text{-}10}$, $rSUV_{max\text{-}15}$, and $rSUV_{max\text{-}20}$. Similarly, the rCBF and minimum ADC values were recorded: $rCBF_{solid}$, $rCBF_5$, $rCBF_{10}$, $rCBF_{15}$ and $rCBF_{20}$; $rADC_{min\text{-}solid}$, $rADC_{min\text{-}5}$, $rADC_{min\text{-}10}$, $rADC_{min\text{-}15}$, and $rADC_{min\text{-}20}$.

Statistical analysis

Statistical analysis was performed on SPSS software (version 26, IBM Corp., Armonk, NY, USA). A P value <0.05 was considered statistically significant.

Continuous variables were expressed as mean ± standard deviation (SD) and compared using independent-sample *t*-tests. Categorical data were expressed as numbers and percentages (%). The interclass correlation coefficient (ICC) was calculated to assess measurement consistency between the 2 radiologists. ICC ≤0.40 indicated poor consistency, 0.40< ICC ≤0.75 medium consistency, and ICC >0.75 high consistency. Kolmogorov-Smirnov tests were used to assess the normality of quantitative data. Imaging parameters across HGG and LGG groups were compared using the 2-sample *t*-test or the Mann-Whitney U test. Receiver operating characteristic (ROC) curves for parameters (single or combined) were used to evaluate their efficiency in discriminating HGGs form LGGs.

An individualized nomogram prediction model was constructed to predict the probability of HGG. The nomogram performance was evaluated by discrimination and calibration. The discriminative ability of the prediction model was determined by concordance index (C-index). A visual calibration plot, comparing the predicted and actual probability of HGG, was performed to calibrate the prediction model. The nomogram was subjected to 1,000 bootstrap resamples for internal validation to assess predictive accuracy (30).

The overall workflow of this study is shown in *Figure 3*.

Results

Demographic characteristics and conventional MRI features

Of the 41 HGGs, 21 had glioblastomas, 13 anaplastic astrocytoma, and 7 anaplastic oligodendroglioma. Among 35 LGGs, 23 had astrocytoma and 12 had oligodendrogliomas. Demographic characteristics and conventional MRI features

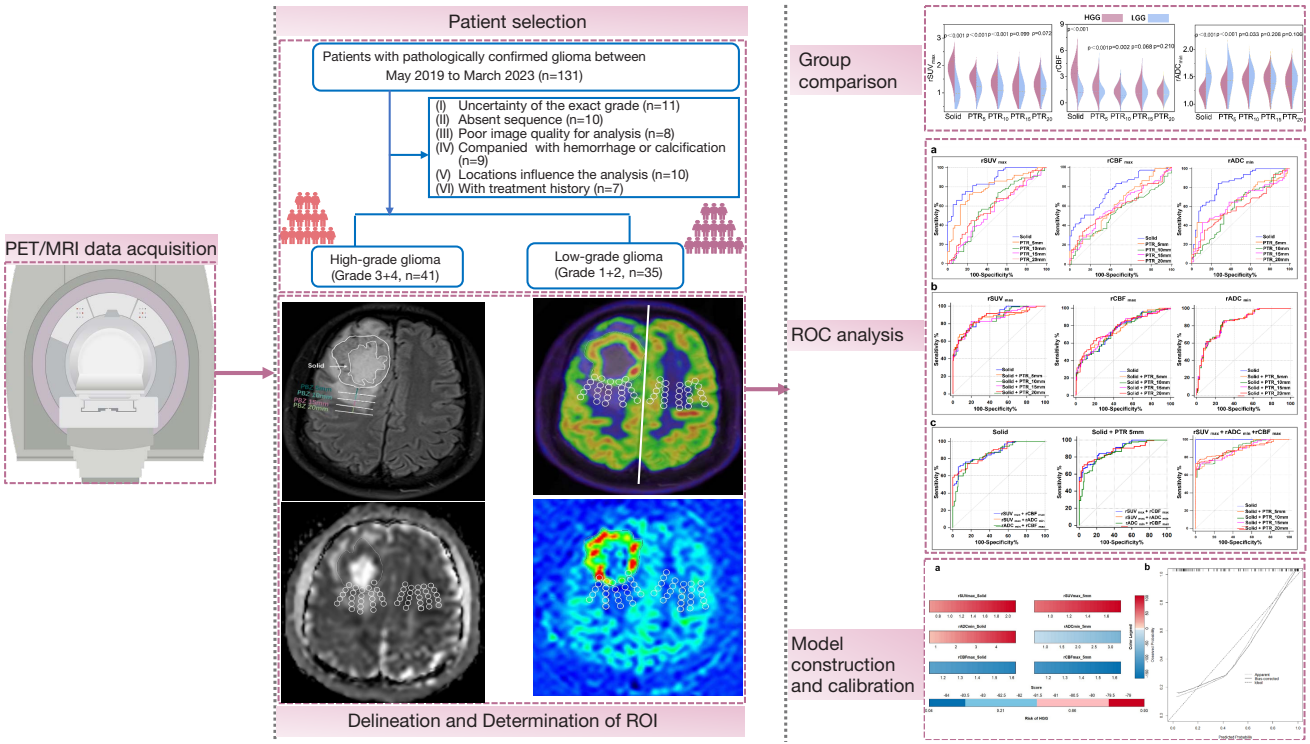

Figure 3 The overall workflow of this study. PET/MRI, positron emission tomography/magnetic resonance imaging; ROI, region of interest; HGG, high-grade glioma; LGG, low-grade glioma; ROC, receiver operating characteristic; $rSUV_{max}$, relative maximum standardized uptake; rCBF, relative cerebral blood flow; $rADC_{min}$, relative minimum apparent diffusion coefficient; PTR, peritumoral region.

are summarized in *Table 1*. Age and sex were comparable across groups.

Interobserver agreement of the multiparametric measurements

The degree of interobserver agreement between the 2 operators for measuring all hybrid PET/MRI parameters were good to excellent (ICC >0.785) (Table S1).

Differences in $rSUV_{max}$, rCBF, and $rADC_{min}$ between HGG and LGG

Detailed and visualized differences in multiparametric measurements between the HGG and LGG groups are presented in Table S2 and *Figure 4*. The HGG group showed a tendency for higher $rSUV_{max}$, lower $rADC_{min}$, and higher rCBF values than did the LGG group, no matter whether there was a statistical difference. Significant inter-group differences were observed mainly in the solid component (all P<0.000, respectively), PTR_5 (P<0.000 for $rSUV_{max}$ and rCBF, P<0.001 for $rADC_{min}$), and PTR_{10} (P<0.000 for $rSUV_{max}$, P=0.011 for $rADC_{min}$, and P=0.002 for rCBF). Examples of patients with HGG and LGG are shown in *Figure 5*.

Diagnostic performance analysis

Diagnostic performance of single parameters

ROC curve analysis indicated that $rSUV_{max\text{-}solid}$ performed the best for grading as a single parameter, with the largest area under the curve (AUC) value of 0.884, followed by $rADC_{min\text{-}solid}$ (0.835) and $rCBF_{solid}$ (0.748). The optimal cut-off value of $rSUV_{max\text{-}solid}$ was 1.388, with a sensitivity and specificity of 87.8% and 85.14%, respectively. The optimal cutoff values, AUC, sensitivity, and specificity are summarized in *Table 2*, whereas the visualized ROC curves are displayed in *Figure 6A*.

Diagnostic performance of combined parameters at different regions

As shown in *Table 3*, when combining the multiparametric

Table 1 Demographic characteristics and conventional MRI features for patients

Variable	HGG (n=41)	LGG (n=35)	P value
Age (years), mean ± SD	51.54±10.54	45.06±12.20	0.299
Gender, n (%)			0.927
Male	18 (43.9)	15 (42.9)	
Female	23 (56.1)	20 (57.1)	
Location (n)			
Frontal lobe	9	7	NA
Parietal lobe	3	5	NA
Temporal lobe	6	4	NA
Occipital lobe	13	13	NA
Multiple lobes	10	6	NA
Cystic degeneration/necrosis, n (%)			0.729
Yes	25 (61.0)	22 (62.9)	
No	16 (39.0)	13 (37.1)	
Mass effect, n (%)			0.107
Yes	17 (41.5)	21 (60.0)	
No	24 (58.5)	14 (40.0)	
IDH mutation, n (%)			0.377
Yes	17 (41.5)	15 (42.9)	
No	18 (43.9)	11 (31.4)	
NOS	6 (14.6)	9 (25.7)	
Type [n]			NA
	Glioblastoma [21]	Astrocytoma [23]	
	Anaplastic astrocytoma [13]	Oligodendroglioma [12]	
	Anaplastic oligodendroglioma [7]		

Statistical significance is indicated by P values less than 0.05. MRI, magnetic resonance imaging; HGG, high-grade glioma; LGG, low-grade glioma; SD, standard deviation; NA, not applicable; IDH, isocitrate dehydrogenase; NOS, not otherwise specified.

indices for the center of the solid component and PTR at distinct distances, the AUC values gradually increased, indicating that the diagnostic performance improved when values for PTR at increased distances were combined. The combination of the $rSUV_{max}$ for the solid component and PTR_{20} showed the largest AUC of 0.881, with sensitivity and specificity values of 0.906 and 0.745, respectively. The visualized curves are shown in *Figure 6B*.

As shown in *Table 4*, when any 2 parameters were combined across DWI, ASL, and ^{18}F FDG-PET for the center of the solid component and PTR_5, the combination of $rSUV_{max}$ with $rADC_{min}$ or rCBF showed equally excellent diagnostic efficacy, with an AUC of 0.874. However, the 3-way combination of parameters from the solid component and PTR_5 had lower AUC values than did the multiparametric combinations for the center only. These visualized curves are shown in *Figure 6C*.

Additionally, when combining all the 3 functional parameters and integrating the parameters from the solid component and PTR at different distances, the discrimination efficacy gradually increased with increasing distance of PTR. The combination of $rSUV_{max}$, $rADC_{min}$,

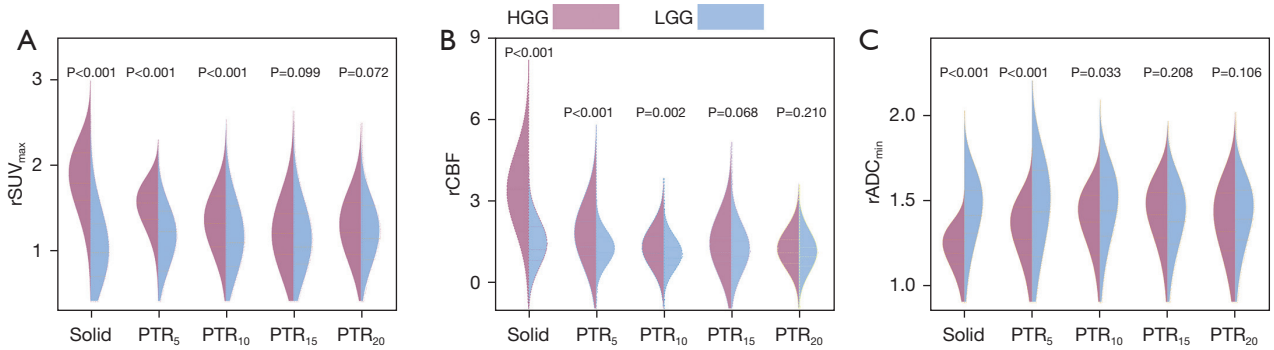

Figure 4 Violin plot of the group differences for the PET, ASL, and DWI parameters. (A) Group differences in $rSUV_{max}$ values. (B) Group differences in rCBF values. (C) Group differences in $rADC_{min}$ values. HGG, high grade glioma; LGG, low grade glioma; $rSUV_{max}$, relative maximum standardized uptake; rCBF, relative cerebral blood flow; $rADC_{min}$, relative minimum apparent diffusion coefficient; PTR, peritumoral region; PET, positron emission tomography; ASL, arterial spin labelling; DWI, diffusion-weighted imaging.

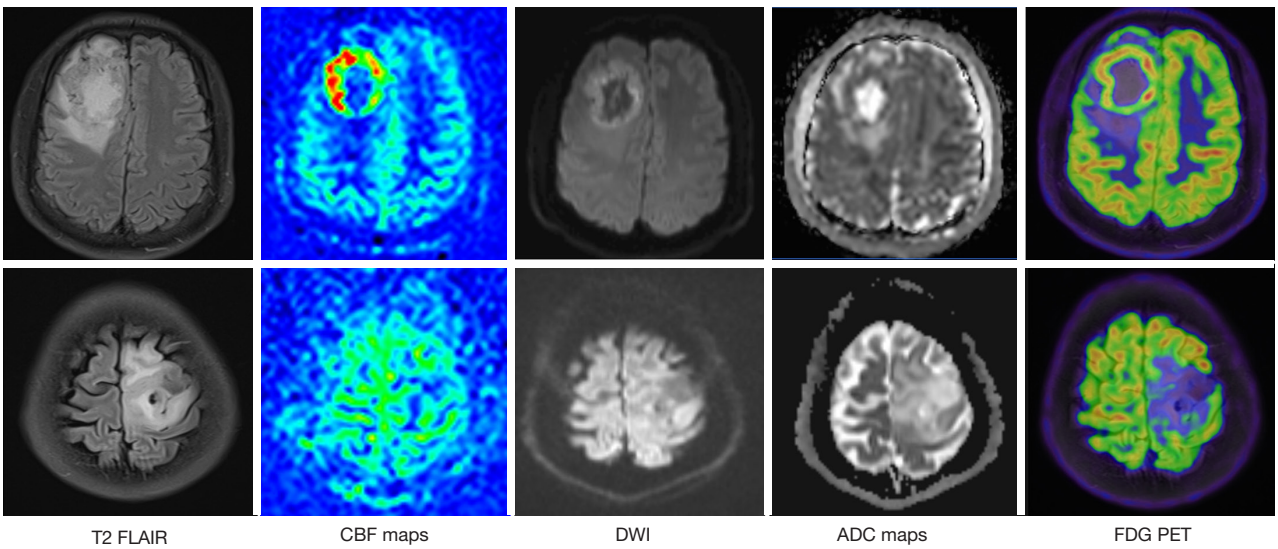

Figure 5 Representative images of the ^{18}F-FDG PET/MRI in patients with HGG and LGG. The first row shows a 34-year-old male patient with HGG. Axial T2-FLAIR image shows a hyperintense mass in the right frontal lobe, with peritumoral edema. The DWI and ADC map demonstrate restricted diffusion both in the solid ($rADC_{min}$ =0.76) of tumor and PTR. The CBF map showed an irregular hyper-perfusion ring (solid, relative cerebral blood flow, rCBF =1.35) but similar CBF in the PTR. The corresponding PET image shows an obvious accumulation of FDG in the solid region (relative maximum standardized uptake, $rSUV_{max}$ =1.26), but decreased uptake in the PTR. The second row shows a 48-year-old female patient with LGG. Axial T2-FLAIR image shows a hyperintense mass located with mild peritumoral edema in left frontal lobe. On the DWI and ADC map, slightly restricted diffusion is observed in the solid of tumor ($rADC_{min}$ =0.98), but not observed in the PTR. The CBF map showed an isoperfusion (rCBF =1.05). The corresponding PET images showed marked decreased uptake of FDG both in the solid ($rSUV_{max}$ =0.85) of tumor and PTR. T2-FLAIR, T2-fuid attenuated inversion recovery; CBF, cerebral blood flow; DWI, diffusion-weighted imaging; ADC, apparent diffusion coefficient; FDG, fluorodeoxyglucose; PET, positron emission tomography; ^{18}F-FDG PET/MRI, ^{18}F-fluorodeoxy glucose positron emission tomography/magnetic resonance imaging; HGG, high-grade glioma; LGG, low-grade glioma; $rSUV_{max}$, relative maximum standardized uptake; rCBF, relative cerebral blood flow; $rADC_{min}$, relative minimum apparent diffusion coefficient; PTR, peritumoral region.

Table 2 Diagnostic performance of single parameter in different tumor regions

Parameters	AUC (95% CI)	Cutoff value	Sensitivity (%)	Specificity (%)	Youden index
$rSUV_{max}$					
Solid	0.884 (0.803–0.927)	1.388	72.7	85.1	0.578
PTR_5	0.775 (0.695–0.862)	1.319	72.2	78.3	0.505
PTR_{10} 10 mm	0.617 (0.497–0.706)	1.178	74.6	49.1	0.238
PTR_{15} 15 mm	0.555 (0.462–0.670)	1.096	64.4	52.7	0.184
PTR_{20} 20 mm	0.548 (0.505–0.708)	1.102	46.3	68.6	0.217
$rADC_{min}$					
Solid	0.835 (0.768–0.910)	0.982	84.4	84.6	0.563
PTR_5	0.659 (0.566–0.760)	0.625	94.3	42.4	0.376
PTR_{10} 10 mm	0.553 (0.495–0.700)	0.799	87.4	36.9	0.225
PTR_{15} 15 mm	0.678 (0.541–0.740)	0.678	42.0	81.1	0.322
PTR_{20} 20 mm	0.624 (0.492–0.695)	0.624	22.9	93.7	0.227
rCBF					
Solid	0.748 (0.680–0.846)	1.080	77.1	59.4	0.387
PTR_5	0.617 (0.516–0.717)	1.131	59.0	56.0	0.193
PTR_{10} 10 mm	0.533 (0.429–0.636)	1.621	25.9	90.9	0.155
PTR_{15} 15 mm	0.597 (0.496–0.698)	1.332	46.3	74.5	0.207
PTR_{20} 20 mm	0.593 (0.491–0.694)	1.761	37.8	91.4	0.222

AUC, area under the curve; CI, confidence interval; $rSUV_{max}$, relative maximum standardized uptake value; PTR_5, the 5-mm PTR; PTR_{10}, the 10-mm PTR; PTR_{15}, the 15-mm PTR; PTR_{20}, the 20-mm PTR; PTR, peritumoral zone; rCBF, relative cerebral blood flow; $rADC_{min}$, relative minimum apparent diffusion coefficient.

and rCBF from the solid component and PTR_{20} had the largest AUC of 0.928, with corresponding sensitivity and specificity were 94.5% and 69.5%, respectively.

Predictive nomogram for the probability of HGG and its performance

According to the diagnostic performance of the combined multi-parameters from different regions, an individualized nomogram prediction model was constructed to predict HGGs (*Figure 7A*). The total score was calculated, including the $rSUV_{max}$, $rADC_{min}$, and rCBF for the solid component and PTR_5, and the value of each variable was assigned a score on the point-scale axis. A total score was calculated by adding each single score. By projecting the total score onto the individual variable axes of the nomogram, we were able to estimate the probability of HGG. The nomogram showed good accuracy, with a C-index of 0.906 [95% confidence interval (CI): 0.849–0.963]. *Figure 7B* displays the calibration curve of the nomogram, which showed that the HGG probabilities predicted by the nomogram agreed well with the actual probabilities.

Discussion

Differentiating LGGs from HGGs can be challenging but essential for making optimal treatment decisions. Recent studies found that glioma cells can infiltrate the apparently normal region covering 20 mm around the tumor border as visualized on conventional enhanced MRI. We proposed to use multiple parameters from solid component and PTRs from hybrid ^{18}F-FDG PET/MRI to grade glioma. HGGs showed higher $rSUV_{max}$, lower $rADC_{min}$, and higher rCBF value relative to LGGs, with significant intergroup differences in $rADC_{min}$ and rCBF values for the solid component and 5–10 mm-adjacent region. Regardless

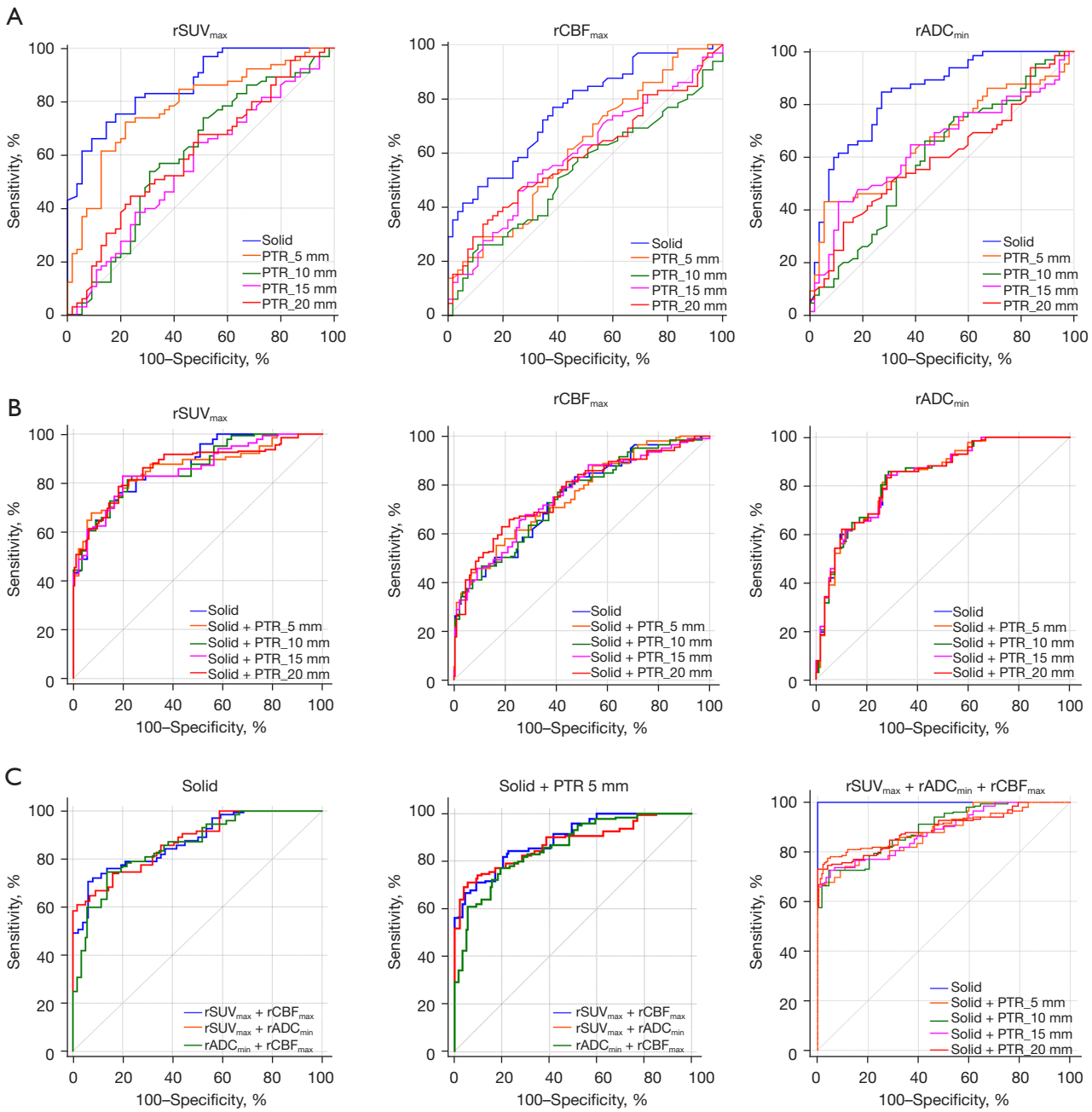

Figure 6 ROC curves of intratumoral solid component and peritumoral regions PET, ASL and DWI parameters for differentiating HGG and LGG. (A) ROC for the $rSUV_{max}$, rCBF and $rADC_{min}$ value as a single parameter for different regions. (B) ROC for the $rSUV_{max}$, rCBF, and $rADC_{min}$ value when combined the solid component and PTR with different distances adjacent to the margin of the solid region. (C) ROC curves for the combination of single, 2 or 3 parameters of $rSUV_{max}$, rCBF, and $rADC_{min}$, and the combination of the solid region with different PTR. $rSUV_{max}$, relative maximum standardized uptake; rCBF, relative cerebral blood flow; $rADC_{min}$, relative minimum apparent diffusion coefficient; PTR, peritumoral region; ROC, receiver operating characteristic; PET, positron emission tomography; ASL, arterial spin labelling; DWI, diffusion-weighted imaging; HGG, high grade glioma; LGG, low grade glioma.

Table 3 Combined diagnostic performance of single parameter with different tumor region

Parameters	AUC (95% CI)	Sensitivity (%)	Specificity (%)	Youden index
$rSUV_{max}$				
Solid	0.865 (0.803–0.927)	71.9	85.5	0.573
PTR_{s+5}	0.860 (0.793–0.927)	67.2	92.7	0.599
PTR_{s+10}	0.864 (0.798–0.929)	81.3	80.0	0.613
PTR_{s+15}	0.868 (0.802–0.934)	82.8	83.6	0.664
PTR_{s+20}	0.881 (0.819–0.943)	90.6	74.5	0.652
$rADC_{min}$				
Solid	0.839 (0.768–0.910)	72.7	84.6	0.573
PTR_{s+5}	0.839 (0.768–0.911)	72.7	84.6	0.573
PTR_{s+10}	0.847 (0.775–0.918)	72.7	96.2	0.589
PTR_{s+15}	0.846 (0.775–0.918)	72.1	86.2	0.589
PTR_{s+20}	0.847 (0.776–0.919)	72.3	84.6	0.573
rCBF				
Solid	0.763 (0.680–0.846)	76.9	61.8	0.387
PTR_{s+5}	0.782 (0.702–0.861)	56.9	85.5	0.424
PTR_{s+10}	0.783 (0.703–0.862)	60.0	87.3	0.473
PTR_{s+15}	0.792 (0.714–0.870)	60.0	87.3	0.473
PTR_{s+20}	0.813 (0.739–0.888)	73.8	78.2	0.529

AUC, area under the curve; CI, confidence interval; $rSUV_{max}$, relative maximum standardized uptake value; PTR_{s+5}, the solid component and the 5-mm PTR; PTR_{s+10}, the solid component and the 10-mm PTR; PTR_{s+15}, the solid component and the 15-mm PTR; PTR_{s+20}, the solid component and the 20-mm PTR; PTR, peritumoral zone; rCBF, relative cerebral blood flow; $rADC_{min}$, relative minimum apparent diffusion coefficient.

of single or combined parameters, only those including $rSUV_{max}$ achieved optimal discrimination performance. When properties of the solid component and PTR at different distances were integrated, the diagnostic efficacy improved with increasing distance of PTR. A nomogram prediction model incorporating 3 parameters from the solid component and PTR, predicted HGGs with optimal discrimination and excellent calibration. This finding is valuable in clinical practice by permitting patients with glioma to be stratified before surgery.

PET provides information on the tumor metabolism and proliferation in a noninvasive, dynamic, qualitative, and quantitative manner. ^{18}F-FDG remains the most widely used radiotracer to evaluate brain tumors, and its uptake indirectly reflects cell density and tumor aggressiveness (31). In the current study, HGGs showed higher $rSUV_{max}$ than did LGGs at any measured point including the solid and PTR; especially in the solid component, the AUC was about 0.803–0.927 in differentiating LGGs from HGGs. This may reflect the high glucose avidity in malignant brain tumors, as suggested in previous reports (18,31,32), ^{18}F-FDG-PET is a reliable tool to reflect this difference. However, these previous studies were mainly performed by combining the MRI and ^{18}F-FDG-PET parameters, rather than hybrid ^{18}F-FDG-PET/MRI-derived parameters. Additionally, we applied a relative SUV_{max}, which may overcome the influence from the background uptake (33) and alleviate some overlap in ^{18}F-FDG uptake to a certain extent. The diagnostic performance in our study was slightly better than that in a previous report (34) in which O-(2-[^{18}F]-fluoroethyl)-L-tyrosine (^{18}F-FET) PET showed an AUC of 0.80–0.83 in differentiating LGGs from HGGs, which may also be ascribed to the relative value applied in this study.

Table 4 Combined diagnostic performance of multiple parameters incorporating multiple tumor regions

Parameters	AUC (95% CI)	Sensitivity (%)	Specificity (%)	Youden index
Solid				
SUV_{max} + ADC_{min}	0.874 (0.815–0.933)	60.0	100	0.600
SUV_{max} + rCBF	0.874 (0.814–0.934)	73.8	94.5	0.684
ADC_{min} + rCBF	0.860 (0.796–0.925)	73.8	87.3	0.611
Solid + PTR_5				
SUV_{max} + ADC_{min}	0.788 (0.705–0.871)	66.2	85.5	0.516
SUV_{max} + rCBF	0.791 (0.710–0.872)	64.6	87.3	0.519
ADC_{min} + rCBF	0.693 (0.599–0.788)	58.5	76.4	0.348
SUV_{max} + ADC_{min} + rCBF				
Solid	0.883 (0.825–0.941)	68.8	10.0	0.688
PTR_{s+5}	0.897 (0.844–0.950)	71.9	94.5	0.664
PTR_{s+10}	0.905 (0.853–0.956)	73.4	94.5	0.680
PTR_{s+15}	0.912 (0.862–0.962)	87.5	71.8	0.693
PTR_{s+20}	0.928 (0.884–0.972)	75.0	94.5	0.695

AUC, area under the curve; CI, confidence interval; PTR, peritumoral region; SUV_{max}, maximum standardized uptake value; ADC_{min}, minimum apparent diffusion coefficient; rCBF, relative cerebral blood flow; PTR_5, the 5-mm PTR; PTR_{s+5}, the solid component and the 5-mm PTR; PTR_{s+10}, the solid component and the 10-mm PTR; PTR_{s+15}, the solid component and the 15-mm PTR; PTR_{s+20}, the solid component and the 20-mm PTR.

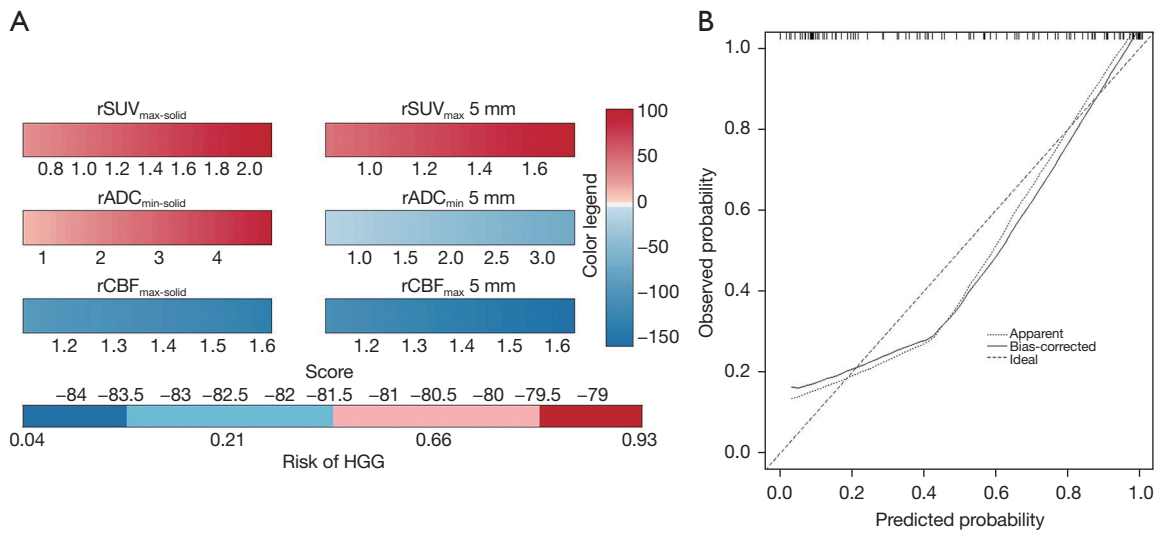

Figure 7 The predictive model of HGG. (A) The visualized predictive nomogram of HGG, incorporating the 3 parameters from the solid component and the peritumoral region ($PTR_{5\ mm}$). The value of each of variable was given a score on the point scale axis. A total score was calculated by adding each single score. By projecting the total score to the lower total point scale, we were able to estimate the probability of HGG. (B) The calibration curves in the nomogram. The x-axis represents the nomogram predicted probability and the y-axis represents the actual probability of HGG. $rSUV_{max}$, relative maximum standardized uptake; $rCBF_{max}$, relative cerebral blood flow; $rADC_{min}$, relative minimum apparent diffusion coefficient; HGG, high-grade glioma; PTR, peritumoral region.

Of note, the HGG and LGG groups differed in the solid component and the 5-mm- and 10-mm-adjacent PTR, suggesting that the greatest metabolic discrepancy between glioma exists mainly in and close to the solid component, where tumor cells proliferate much more actively. This was in line with the theoretical tumor region mode that with the increasing of the distance adjacent to the PTR, the tumor cell density decreased (35). Although there was no between-group difference, $rSUV_{max}$ in the 15–20-mm-adjacent PTR (Table S2 and *Figure 4A*) exhibited some alterations, indicating occult metabolic abnormality in the PTR that was considered normative in past decades. Therefore, PTR is an important area that should not be undervalued in the evaluation of gliomas. Importantly, compared to relying on a single parameter from any imaging technique or any tumor region, incorporating $rSUV_{max}$ with other MRI (DWI or ASL) parameters enhances grading performance. Thus, $rSUV_{max}$ plays a significant role in differentiation of glioma grades. This research agrees with a previous review reporting that ^{18}F-FDG PET can provide additional information that complements MRI data, thus easing glioma management (18). In this context, we consider that ^{18}F-FDG-PET/MRI can be a vital step in the clinical workflow to distinguish HGGs from LGGs before surgery.

ASL provides microcirculation information by measuring blood flow using magnetically labeled water protons in the arterial blood as an endogenous tracer. rCBF derived from ASL has been viewed as an effective marker for discriminating LGGs from HGGs (36,37); however, it has not been used to assess PTR for glioma grading. In our study, a puzzling result was that rCBF values were higher for HGGs than for LGGs even at areas located 20 mm away from the tumor margin. However, this is not sufficient to distinguish the 2 grades. We suggest that there is aberrant vascularization in a wide area of PTR in both HGGs and LGGs. This could be attributed to the tumorigenic and angiogenic properties of PTR, which promote the growth and invasion of gliomas (38). In a pilot study, it may be worth assessing the merits of rCBF values at 15–20 mm from the conventionally defined tumor margins as a sensitivity marker for PTR. DWI-generated ADC values can quantitatively evaluate tissue cellularity, which is useful because proliferating tumor cells hamper extracellular water diffusion *in vivo* (39). Nevertheless, the grading performance of PTR based on ADC has not been scrutinized. Our findings revealed significantly decreased $rADC_{min}$ values for HGGs, consistent with the results of previous studies (40). Similar to the findings in a previous report (26), we found an increase in the $rADC_{min}$ in PTR, and, with increasing distance of PTR, the $rADC_{min}$ values also decreased; however, the properties of PTR have not been studied in detail.

Multiparametric imaging is a promising tool for distinguishing tumor characteristics. ^{18}F-FDG PET/MRI not only provides glucose metabolism information via ^{18}F-FDG PET imaging but also enables the simultaneous acquisition of multiple quantitative MRI during PET imaging, providing a more comprehensive assessment of the glioma grading. Our study verified that a combination of multiple parameters derived from ^{18}F FDG-PET/MRI ($rSUV_{max}$, $rADC_{min}$, or rCBF) yielded better results than did use of a single parameter or incorporation of any 2 parameters alone. In particular, those including $rSUV_{max}$ achieved optimal discrimination performance; our results further supported the recommendation of the Neuro-Oncology working group for the clinical use of PET imaging in glioma (32). These findings suggest that integrated PET/MRI may be particularly useful for grading gliomas, providing comprehensive morphological and metabolic information in a single examination. Furthermore, a single ^{18}F-FDG PET/MRI examination was less influenced by the unaligned images from multimodality images, providing a robust result (41).

Interestingly, when the 3 ^{18}FDG-PET/MRI-based parameters were combined for distinct tumor regions, the combination of parameters derived from the solid component of the tumor and PTR_{20} displayed the best performance in differentiating HGGs form LGGs, with an AUC of 0.928 (95% CI: 0.884–0.972). Pallud *et al.* (42) collected biopsy samples within and beyond tumor margins, finding a significant density of tumor cells at distances of 10–20 mm beyond the conventional imaging-defined limits. Similarly, Gerin *et al.* (43) discovered tumor cell infiltration in up to 20 mm of parenchyma around conventional MRI-defined abnormalities. However, the aforementioned MRI acquisition protocols were mostly performed using conventional MRI sequences such as T2WI. Zhang *et al.* (28) reported that a multiparametric measurement of the enhancing tumors and PTR diagnostic model based on ^{18}F-FDG PET/MRI is superior to a single parameter method in differentiating of HGG from the primary central nervous system lymphoma. Thus, our nomogram may be an important predictive tool to determine patient-specific probabilities of HGGs with optimal discrimination, with a C-index of 0.906 (95% CI: 0.849–0.963).

Our study had several limitations. First, this was a single-

center, retrospective study with a small sample size. We could not separate subgroups, such as according to IDH mutation and other characteristics, as this would have reduced statistical power. Thus, the results may have been statistically biased. A large cohort from multiple centers is required for validation. Second, this retrospective study was conducted from 2019. As a result, the pathological results of the included samples were based on the 2016 CNS WHO classification (4th edition) instead of the latest edition (5th edition) released in 2021. Third, multiparametric measures for PTR do not provide direct evidence regarding the histopathology of the tumor tissue. This is also a clinical challenge that may be overcome to some degree by conducting animal studies. Fourth, due to ethical constraints by the Internal Ethics Committee of the Hospital, we could not perform both FDG and FET-PET for evaluation, although some reports have mentioned that the ^{18}F-FET possessed some advantages over ^{18}F-FDG-PET. Meanwhile, a systematic review and meta-analysis (22) found that both tracers were able to distinguish between LGGs and HGGs. Furthermore, we used the relative value of the SUV_{max}, which may alleviate the disadvantage of the ^{18}F-FDG to some degree.

Conclusions

The combination of $rSUV_{max}$, rCBF, and $rADC_{min}$ derived from hybrid PET/MRI of the solid component and PTR facilitated more accurate discrimination of LGGs from HGGs than did a single parameter alone. ^{18}F-FDG PET/MRI has particular value in estimating the glioma histologic grade, which is a potential tool to guide the initiation of proper treatment and improve patients' outcomes. Thus, multiparametric ^{18}F-FDG PET/MRI can be a vital step in the clinical workflow to distinguish HGGs from LGGs before surgery. Moreover, the cellular and metabolic features of PTR in both HGGs and LGGs are crucial for identifying new therapeutic targets (25).

Acknowledgments

Part of the results in this article was submitted to 2023 RSNA and accepted as oral presentation (abstract #14105).
Funding: This work was supported by the National Natural Science Foundation of China (No. 82102004 to P.L. and No. 82271948 to G.H.J.), Science and Technology Planning Project of Guangzhou (No. 2023A03J0276 to P.L.), and the Key Laboratory Construction Project of the Guangzhou Science and Technology (No. 202201020373 to G.H.J.).

Footnote

Reporting Checklist: The authors have completed the TRIPOD reporting checklist. Available at https://qims.amegroups.com/article/view/10.21037/qims-24-280/rc

Conflicts of Interest: All authors have completed the ICMJE uniform disclosure form (available at https://qims.amegroups.com/article/view/10.21037/qims-24-280/coif). P.L. reports a grant from the Science and Technology Planning Project of Guangzhou (No. 2023A03J0276) and the National Natural Science Foundation of China (No. 82102004) during the conduct of the study. G.H.J. reports a grant from the National Natural Science Foundation of China (No. 82271948) and the Key Laboratory Construction Project of the Guangzhou Science and Technology (No. 202201020373) during the conduct of the study. The other authors have no conflicts of interest to declare.

Ethical Statement: The authors are accountable for all aspects of the work in ensuring that questions related to the accuracy or integrity of any part of the work are appropriately investigated and resolved. The study was conducted in accordance with the Declaration of Helsinki (as revised in 2013) and approved by the Institutional Review Board of Guangzhou Universal Medical Imaging Diagnostic Center (No. 003/2019). All patients signed an informed consent form for the 18F-FDG PET/MRI examination. The data applied in this study were exempted from ethical review due to the retrospective nature.

References

1. He Y, Cai Y, Liu J, Ding H, Li X, Tian S, Li Z. Systematic Analysis of a Pyroptosis-Related Signature to Predict the

Prognosis and Immune Microenvironment of Lower-Grade Glioma. Cells 2022;11:3980.
2. Louis DN, Perry A, Wesseling P, Brat DJ, Cree IA, Figarella-Branger D, Hawkins C, Ng HK, Pfister SM, Reifenberger G, Soffietti R, von Deimling A, Ellison DW. The 2021 WHO Classification of Tumors of the Central Nervous System: a summary. Neuro Oncol 2021;23:1231-51.
3. McNamara C, Mankad K, Thust S, Dixon L, Limback-Stanic C, D'Arco F, Jacques TS, Löbel U. 2021 WHO classification of tumours of the central nervous system: a review for the neuroradiologist. Neuroradiology 2022;64:1919-50.
4. Ostrom QT, Cioffi G, Gittleman H, Patil N, Waite K, Kruchko C, Barnholtz-Sloan JS. CBTRUS Statistical Report: Primary Brain and Other Central Nervous System Tumors Diagnosed in the United States in 2012-2016. Neuro Oncol 2019;21:v1-v100.
5. Gu W, Fang S, Hou X, Ma D, Li S. Exploring diagnostic performance of T2 mapping in diffuse glioma grading. Quant Imaging Med Surg 2021;11:2943-54.
6. Du N, Shu W, Li K, Deng Y, Xu X, Ye Y, Tang F, Mao R, Lin G, Li S, Fang X. An initial study on the predictive value using multiple MRI characteristics for Ki-67 labeling index in glioma. J Transl Med 2023;21:119.
7. Martucci M, Russo R, Schimperna F, D'Apolito G, Panfili M, Grimaldi A, Perna A, Ferranti AM, Varcasia G, Giordano C, Gaudino S. Magnetic Resonance Imaging of Primary Adult Brain Tumors: State of the Art and Future Perspectives. Biomedicines 2023;11:364.
8. Guida L, Stumpo V, Bellomo J, van Niftrik CHB, Sebök M, Berhouma M, Bink A, Weller M, Kulcsar Z, Regli L, Fierstra J. Hemodynamic Imaging in Cerebral Diffuse Glioma-Part A: Concept, Differential Diagnosis and Tumor Grading. Cancers (Basel) 2022;14:1432.
9. Lindner T, Bolar DS, Achten E, Barkhof F, Bastos-Leite AJ, Detre JA, et al. Current state and guidance on arterial spin labeling perfusion MRI in clinical neuroimaging. Magn Reson Med 2023;89:2024-47.
10. Alkanhal H, Das K, Poptani H. Diffusion- and Perfusion-Weighted Magnetic Resonance Imaging Methods in Nonenhancing Gliomas. World Neurosurg 2020;141:123-30.
11. Hales PW, d'Arco F, Cooper J, Pfeuffer J, Hargrave D, Mankad K, Clark C. Arterial spin labelling and diffusion-weighted imaging in paediatric brain tumours. Neuroimage Clin 2019;22:101696.
12. Hashido T, Saito S, Ishida T. Radiomics-Based Machine Learning Classification for Glioma Grading Using Diffusion- and Perfusion-Weighted Magnetic Resonance Imaging. J Comput Assist Tomogr 2021;45:606-13.
13. Roach JR, Plaha P, McGowan DR, Higgins GS. The role of [18F]fluorodopa positron emission tomography in grading of gliomas. J Neurooncol 2022;160:577-89.
14. Zhang-Yin JT, Girard A, Bertaux M. What Does PET Imaging Bring to Neuro-Oncology in 2022? A Review. Cancers (Basel) 2022;14:879.
15. Çelebi F, Yaghouti K, Cindil E, Dogusoy GB, Tokat Y, Balcı C. The Role of 18F-FDG PET/MRI in the Assessment of Primary Intrahepatic Neoplasms. Acad Radiol 2021;28:189-98.
16. Almansory KO, Fraioli F. Combined PET/MRI in brain glioma imaging. Br J Hosp Med (Lond) 2019;80:380-6.
17. Overcast WB, Davis KM, Ho CY, Hutchins GD, Green MA, Graner BD, Veronesi MC. Advanced imaging techniques for neuro-oncologic tumor diagnosis, with an emphasis on PET-MRI imaging of malignant brain tumors. Curr Oncol Rep 2021;23:34.
18. Quartuccio N, Laudicella R, Vento A, Pignata S, Mattoli MV, Filice R, Comis AD, Arnone A, Baldari S, Cabria M, Cistaro A. The Additional Value of (18)F-FDG PET and MRI in Patients with Glioma: A Review of the Literature from 2015 to 2020. Diagnostics (Basel) 2020;10:357.
19. Ferda J, Ferdová E, Hes O, Mraček J, Kreuzberg B, Baxa J. PET/MRI: Multiparametric imaging of brain tumors. Eur J Radiol 2017;94:A14-25.
20. Katsanos AH, Alexiou GA, Fotopoulos AD, Jabbour P, Kyritsis AP, Sioka C. Performance of 18F-FDG, 11C-Methionine, and 18F-FET PET for Glioma Grading: A Meta-analysis. Clin Nucl Med 2019;44:864-9.
21. Yoon JH, Kim JH, Kang WJ, Sohn CH, Choi SH, Yun TJ, Eun Y, Song YS, Chang KH. Grading of cerebral glioma with multiparametric MR imaging and 18F-FDG-PET: concordance and accuracy. Eur Radiol 2014;24:380-9.
22. Dunet V, Pomoni A, Hottinger A, Nicod-Lalonde M, Prior JO. Performance of 18F-FET versus 18F-FDG-PET for the diagnosis and grading of brain tumors: systematic review and meta-analysis. Neuro Oncol 2016;18:426-34.
23. Giambra M, Messuti E, Di Cristofori A, Cavandoli C, Bruno R, Buonanno R, Marzorati M, Zambuto M, Rodriguez-Menendez V, Redaelli S, Giussani C, Bentivegna A. Characterizing the Genomic Profile in High-Grade Gliomas: From Tumor Core to Peritumoral Brain Zone, Passing through Glioma-Derived Tumorspheres. Biology (Basel) 2021;10:1157.
24. Lemée JM, Clavreul A, Aubry M, Com E, de Tayrac

M, Eliat PA, Henry C, Rousseau A, Mosser J, Menei P. Characterizing the peritumoral brain zone in glioblastoma: a multidisciplinary analysis. J Neurooncol 2015;122:53-61.
25. Silva M, Vivancos C, Duffau H. The Concept of «Peritumoral Zone» in Diffuse Low-Grade Gliomas: Oncological and Functional Implications for a Connectome-Guided Therapeutic Attitude. Brain Sci 2022;12:504.
26. Pauleit D, Langen KJ, Floeth F, Hautzel H, Riemenschneider MJ, Reifenberger G, Shah NJ, Müller HW. Can the apparent diffusion coefficient be used as a noninvasive parameter to distinguish tumor tissue from peritumoral tissue in cerebral gliomas? J Magn Reson Imaging 2004;20:758-64.
27. Jensen RL, Mumert ML, Gillespie DL, Kinney AY, Schabel MC, Salzman KL. Preoperative dynamic contrast-enhanced MRI correlates with molecular markers of hypoxia and vascularity in specific areas of intratumoral microenvironment and is predictive of patient outcome. Neuro Oncol 2014;16:280-91.
28. Zhang S, Wang J, Wang K, Li X, Zhao X, Chen Q, Zhang W, Ai L. Differentiation of high-grade glioma and primary central nervous system lymphoma: Multiparametric imaging of the enhancing tumor and peritumoral regions based on hybrid (18)F-FDG PET/MRI. Eur J Radiol 2022;150:110235.
29. Alsaedi A, Doniselli F, Jäger HR, Panovska-Griffiths J, Rojas-Garcia A, Golay X, Bisdas S. The value of arterial spin labelling in adults glioma grading: systematic review and meta-analysis. Oncotarget 2019;10:1589-601.
30. Jin C, Cao J, Cai Y, Wang L, Liu K, Shen W, Hu J. A nomogram for predicting the risk of invasive pulmonary adenocarcinoma for patients with solitary peripheral subsolid nodules. J Thorac Cardiovasc Surg 2017;153:462-469.e1.
31. Song PJ, Lu QY, Li MY, Li X, Shen F. Comparison of effects of 18F-FDG PET-CT and MRI in identifying and grading gliomas. J Biol Regul Homeost Agents 2016;30:833-8.
32. Albert NL, Weller M, Suchorska B, Galldiks N, Soffietti R, Kim MM, la Fougère C, Pope W, Law I, Arbizu J, Chamberlain MC, Vogelbaum M, Ellingson BM, Tonn JC. Response Assessment in Neuro-Oncology working group and European Association for Neuro-Oncology recommendations for the clinical use of PET imaging in gliomas. Neuro Oncol 2016;18:1199-208.
33. Smeraldo A, Ponsiglione AM, Soricelli A, Netti PA, Torino E. Update on the Use of PET/MRI Contrast Agents and Tracers in Brain Oncology: A Systematic Review. Int J Nanomedicine 2022;17:3343-59.
34. Verger A, Filss CP, Lohmann P, Stoffels G, Sabel M, Wittsack HJ, Kops ER, Galldiks N, Fink GR, Shah NJ, Langen KJ. Comparison of (18)F-FET PET and perfusion-weighted MRI for glioma grading: a hybrid PET/MR study. Eur J Nucl Med Mol Imaging 2017;44:2257-65.
35. Eyüpoglu IY, Buchfelder M, Savaskan NE. Surgical resection of malignant gliomas-role in optimizing patient outcome. Nat Rev Neurol 2013;9:141-51.
36. Ningning D, Haopeng P, Xuefei D, Wenna C, Yan R, Jingsong W, Chengjun Y, Zhenwei Y, Xiaoyuan F. Perfusion imaging of brain gliomas using arterial spin labeling: correlation with histopathological vascular density in MRI-guided biopsies. Neuroradiology 2017;59:51-9.
37. White CM, Pope WB, Zaw T, Qiao J, Naeini KM, Lai A, Nghiemphu PL, Wang JJ, Cloughesy TF, Ellingson BM. Regional and voxel-wise comparisons of blood flow measurements between dynamic susceptibility contrast magnetic resonance imaging (DSC-MRI) and arterial spin labeling (ASL) in brain tumors. J Neuroimaging 2014;24:23-30.
38. Lo Greco MC, Milazzotto R, Liardo RLE, Acquaviva G, La Rocca M, Altieri R, Certo F, Barbagallo GM, Basile A, Foti PV, Palmucci S, Pergolizzi S, Pontoriero A, Spatola C. Relapsing High-Grade Glioma from Peritumoral Zone: Critical Review of Radiotherapy Treatment Options. Brain Sci 2022;12:416.
39. Chawla S, Krejza J, Vossough A, Zhang Y, Kapoor GS, Wang S, O'Rourke DM, Melhem ER, Poptani H. Differentiation between oligodendroglioma genotypes using dynamic susceptibility contrast perfusion-weighted imaging and proton MR spectroscopy. AJNR Am J Neuroradiol 2013;34:1542-9.
40. Yang X, Xing Z, She D, Lin Y, Zhang H, Su Y, Cao D. Grading of IDH-mutant astrocytoma using diffusion, susceptibility and perfusion-weighted imaging. BMC Med Imaging 2022;22:105.
41. Shang F, Tan Z, Gong T, Tang X, Sun H, Liu S. Evaluation of parametrial infiltration in patients with IB-IIB cervical cancer by a radiomics model integrating features from tumoral and peritumoral regions in (18) F-fluorodeoxy glucose positron emission tomography/MR images. NMR Biomed 2023. [Epub ahead of print]. doi: 10.1002/nbm.4945.
42. Pallud J, Varlet P, Devaux B, Geha S, Badoual M, Deroulers C, Page P, Dezamis E, Daumas-Duport C, Roux

FX. Diffuse low-grade oligodendrogliomas extend beyond MRI-defined abnormalities. Neurology 2010;74:1724-31.
43. Gerin C, Pallud J, Deroulers C, Varlet P, Oppenheim C, Roux FX, Chrétien F, Thomas SR, Grammaticos B, Badoual M. Quantitative characterization of the imaging limits of diffuse low-grade oligodendrogliomas. Neuro Oncol 2013;15:1379-88.

Cite this article as: Liu P, Zeng YP, Qu H, Zheng WY, Zhou TX, Hang LF, Jiang GH. Multiparametric simultaneous hybrid ^{18}F-fluorodeoxyglucose positron emission tomography/magnetic resonance imaging (^{18}F-FDG PET/MRI) incorporating intratumoral and peritumoral regions for grading of glioma. Quant Imaging Med Surg 2024;14(8):5665-5681. doi: 10.21037/qims-24-280

